1 *Rapid, concurrent formation of organic sulfur and iron sulfides during experimental sulfurization of*

2 *sinking marine particles*

3 M. R. Raven[1*], R. G. Keil[2], S. M. Webb[3]

4 [1] Department of Earth Science, University of California, Santa Barbara, Santa Barbara CA 93117, USA

5 [2] School of Oceanography, University of Washington, Seattle WA 98195, USA

6 [3] Stanford Synchrotron Radiation Lightsource, Stanford University, Menlo Park CA 94025, USA

7

8 **Key Points:**
9 **1.** Organic matter in sinking marine particles, and especially apparent EPS, sulfurizes rapidly in the
10 presence of environmentally relevant concentrations polysulfides, tripling its S:C ratio.
11 **2.** Diffuse iron monosulfides form from iron oxyhydroxide particles on the same timescale as organic
12 sulfur.
13 **3.** Organic matter sulfurization in sinking particles has the potential to increase carbon burial in
14 underlying sediments, impacting sedimentary records and climate.

Abstract

Organic matter (OM) sulfurization can enhance the preservation and sequestration of carbon in anoxic sediments, and it has been observed in sinking marine particles from marine O_2-deficient zones. The magnitude of this effect on carbon burial remains unclear, however, because the transformations that occur when sinking particles encounter sulfidic conditions remain undescribed. Here, we briefly expose sinking marine particles from the eastern tropical North Pacific O_2-deficient zone to environmentally relevant sulfidic conditions (20°C, 0.5 mM [poly]sulfide, two days) and then characterize the resulting solid-phase organic and inorganic products in detail. During these experiments, the abundance of organic sulfur in both hydrolyzable and hydrolysis-resistant solids roughly triples, indicating extensive OM sulfurization. Lipids also sulfurize on this timescale, albeit less extensively. In all three pools, OM sulfurization produces organic sulfides, thiols, and disulfides. Hydrolyzable sulfurization products appear within diffuse, ≤ 200-μm regions that are suggestive of sulfurized extracellular polymeric substances (EPS). Concurrently, reactions with particulate iron oxyhydroxides generate diffuse iron sulfide (FeS). Iron oxyhydroxides were not fully consumed during the experiment, which demonstrates that organic materials can be competitive with reactive iron for sulfide. These experiments support the hypothesis that sinking particulate OM in a sulfidic ocean can sulfurize within days. Both iron monosulfides and initial OM sulfurization products may undergo subsequent transformations into more stable forms for long-term preservation, which could impact their speciation and S-isotope composition. OM- and EPS-rich particles that encounter sulfidic conditions in the environment can sulfurize rapidly and are likely to contribute to enhanced sedimentary carbon sequestration.

1. Introduction

In most of the surface ocean today, photosynthetic algae and bacteria produce organic matter (OM) that is cycled efficiently and locally through metabolic networks linking bacteria, viruses, zooplankton, and

2

40 their exudates. OM may also become incorporated into aggregates with sufficient density to sink, or it can

41 be transported out of the mixed layer by other particle "pumps" (Boyd et al., 2019). Large ($\geq$ ~1 mm),

42 sinking particles may travel thousands of meters to the seafloor in a few days (La Rocha and Passow, 2007).

43 As particles sink, they are continually used as a food source, so the downward flux of sinking particulate

44 OM is strongly attenuated with depth due to oxic respiration. As a result, only a tiny fraction (~1.5%) of

45 global marine primary production is buried in sediments. In contrast, the efficiency of OM burial can be

46 much higher in certain types of near-shore (coastal, shelf, or borderland basin) environments (Dunne et al.,

47 2007; Bianchi et al., 2018), especially those with low dissolved O_2 concentrations like the O_2-deficient

48 zones (ODZs) of the Eastern Tropical Pacific and Arabian Sea (Martin et al., 1987; Devol and Hartnett,

49 2001; B. Van Mooy et al., 2002; Hartnett and Devol, 2003). Under the more strongly reducing, frequently

50 sulfidic conditions found in the southern North Atlantic during the Cretaceous ocean anoxic events, OM

51 burial in sediments served as a major sink for CO_2 and likely mitigated a hothouse climate (Arthur et al.,

52 1988; Sinninghe Damsté and Köster, 1998; Hülse et al., 2019). Nonetheless, without a more mechanistic

53 understanding of the underlying causes of enhanced sinking particle fluxes in anoxic environments, we are

54 unable to quantitatively predict how ongoing ODZ expansion and other changes in marine O_2 availability

55 (Deutsch et al., 2011; Stramma et al., 2011; Schmidtko et al., 2017; Breitburg et al., 2018; Takano et al.,

56 2018) will impact carbon fluxes to the sediments.

57   Multiple physical, chemical, and biological mechanisms contribute to the enhanced sinking organic

58 particle flux through anoxic water columns (Keil et al., 2016). Especially in anoxic environments, clays and

59 other minerals physically protect sedimentary OM by occlusion or sorption onto surfaces (Salmon et al.,

60 2000; Arnarson and Keil, 2007). Anaerobic microorganisms also gain less energy from the oxidation of

61 organic matter than aerobic organisms (Froelich et al., 1979), and some individual organic molecules may

62 become energetically inaccessible at certain redox potentials (Boye et al., 2017). However, anoxic

63 sedimentary systems often preserve greater quantities of OM than can be explained by surface protection,

64 microbial energetics, or the availability of alternative electron acceptors like sulfate (Arndt et al., 2013),

65 indicating that there is a role for condensation and kerogenization reactions that render OM inaccessible to

66 microbes and their exoenzymes. A special category of kerogenization reactions that is specific to anoxic

67 environments, OM sulfurization, was observed in sinking ODZ particles under *in-situ* conditions and could

68 be a significant contributor to OM burial (Raven et al., 2021).

69   OM sulfurization reduces the effective lability of OM by replacing certain functional groups (e.g.,

70 aldehydes, conjugated double bonds) with organic S functionalities and by bridging molecules together,

71 increasing their molecular weight (Damsté et al., 1988; Kohnen et al., 1989; Kutuzov et al., 2019).

72 Sulfurized OM is thus less susceptible to breakdown by microbial exoenzymes than fresh or degraded algal

73 biomass (Boussafir and Lallier-Verges, 1997; Sinninghe Damsté and Köster, 1998). The reactants for

74 sulfurization on timescales of days or less appear to be polysulfides (S_x^{2-}, $2 \leq x \leq 8$), which form

75 spontaneously in the presence of dissolved sulfide (HS^-) and elemental S (S^0) or other oxidants (Kamyshny

76 et al., 2004; Rickard and Luther, 2007). In experiments, algal biomass has been shown to sulfurize rapidly

77 in the presence of dissolved polysulfides, producing pyrolysates interpreted as deriving from carbohydrates

78 cross-linked with organic sulfides and polysulfides (Gelin et al., 1998; Kok, Schouten, et al., 2000;

79 Pohlabeln et al., 2017). Experiments with model compounds have shown similar cross-linking following

80 polysulfide exposure (van Dongen et al., 2003; Amrani and Aizenshtat, 2004a). Over the past few years,

81 OM sulfurization has been reported across a growing diversity of environments, including coastal mangrove

82 forests, hydrothermal systems, marine surface sediments exposed to variable redox conditions (Gomez-

83 Saez et al., 2016; Jessen et al., 2017; Raven, Fike, Gomes, et al., 2019), and sinking marine particles in both

84 sulfidic basins and anoxic (non-sulfidic) ODZs (Raven, Sessions, Adkins, et al., 2016; Raven et al., 2021).

85 The sulfurization of OM in sinking marine particles could have a particularly large effect on fluxes in the

86 marine carbon cycle because it impacts a relatively large and reactive pool of sinking biomass, where

87 moderate changes in preservation efficiency can translate into substantial changes in the rates of

88 sedimentary OM burial (Raven et al., 2018).

89   In this study, we investigate how sinking marine particles from the eastern tropical North Pacific

90   ODZ respond to a brief exposure to environmentally relevant sulfidic conditions. The 48-hour duration of

91   these experiments could be analogous to, for example, the experience of a large particle sinking through a

92   polysulfide-rich chemocline in the water column. Previous sulfurization experiments that demonstrated

93   rapid OM sulfurization generally used model compounds (Amrani and Aizenshtat, 2004b) or elevated

94   temperatures, phase transfer agents, and/or elevated polysulfide concentrations that make them challenging

95   to directly compare with modern marine environments (e.g., 50°C, 13 mM [poly]sulfide, 30 days) (Gelin

96   et al., 1998; Kok, Rijpstra, et al., 2000; van Dongen et al., 2003). Here, we conduct two-day experiments

97   with natural particle samples under environmental conditions (20°C, 0.5 mM [poly]sulfide), and use an

98   expanded suite of x-ray spectroscopic techniques, to investigate how sulfidic conditions transform sinking

99   marine particles.

100

101   **2. Materials and Methods**

102

103   *2.1 Sampling site*

104   Samples were collected from the eastern tropical North Pacific ODZ in spring 2018 as part of cruise

105   RR1807 on the R/V Roger Revelle. We deployed a surface-float-tethered particle trap with a 2-meter-

106   diameter, 50-μm-mesh net (Van Mooy and Keil, 2015) at two sites: a relatively low particle flux site ('P2,'

107   200 km from the Mexican coast, 17.0°N x 107.0°W, ~3500 m water depth), and a relatively high particle

108   flux site ('P1,' ~50 km from shore, 20.3°N x 106.1°W, ~1500 m water depth). This same population of

109   samples was previously used for radiosulfur measurements of microbial sulfate reduction rates and the

110   identification of *in-situ* organic S formation (Raven et al., 2021). Particles were trapped at the depth of the

111   secondary nitrite maximum (120-143 m at P1 and 147 m at P2) for approximately 48 hrs. After recovery,

112   the 2-m-diameter net, which closed *in-situ* before recovery, was rinsed with filtered surface seawater to

113   collect particles. Samples for this study (Table S1) include one sample from P2 ('F') and five samples from

114 P1 ('A' through 'E'), all of which were collected from the 'net wash.' During processing, the experimental

115 sample from P2 was lost due to an unfortunate wind incident. Aliquots for controls ('A_C,' 'B_C,' etc.) were

116 syringe-filtered in a N_2-filled glovebag onto pre-combusted, 0.7 μm (GF-F) glass fiber filters and

117 immediately frozen under N_2 headspace at –20°C. Aliquots for polysulfide exposure experiments ('A_{Sx},',

118 B_{Sx},' etc.) were transferred to 250-mL serum bottles and sparged with N_2. Each experiment received 10 mL

119 of a 12-mM, filtered, ^{34}S-labeled, mixed sulfide-polysulfide solution yielding a total reduced sulfur

120 concentration in experiments of 0.52 mM. Label solutions were prepared at pH 8 and in the presence of

121 excess S^0(s), which means that the reactant pool was initially composed of roughly half bisulfide (HS$^-$) and

122 half polysulfides (S_x^{2-}) (Rickard and Luther, 2007). Bottles were incubated for 48 hrs at ~20°C in the dark.

123 After incubation, 1-mL aliquots of seawater were filtered through GF-F filters into vials containing

124 concentrated HCl to volatilize H_2S and then preserved with $BaCl_2$ for sulfate S-isotope analysis. Particle

125 solids were collected anoxically onto pre-combusted GF-F filters and frozen under N_2 at –20°C.

126   *2.2 Sample collection, handling, and processing*

127   Particle samples were subdivided into three pools for analysis: extractable lipids (OM$_{Lipid}$), acid-

128 soluble/volatile materials (OM$_{Hyd}$), and acid-resistant organics (OM$_{Res}$). After filters were washed with N_2-

129 sparged pH 7.8 tris buffer solution to remove inorganic sulfate and lyophilized, splits were set aside for

130 'whole particle' spectroscopy, and selected controls with sufficient particle material were split to allow

131 elemental and isotopic analysis of 'whole particles' with minimal disruption. Remaining particles were

132 microwave-extracted (CEM MARS-6) twice in 9:1 dichloromethane:methanol. Solvent extracts were

133 concentrated under N_2 and exposed to activated Cu^0 for 12 hrs to remove elemental S. Lipid extract aliquots

134 for XAS were dried onto quartz slides, and the remaining material was trapped onto washed and dried silica

135 gel for elemental analysis. Splits of solvent-extracted particle filters were set aside for x-ray absorption

136 spectroscopy and x-ray fluorescence mapping (XAS/XRF), and experimental samples with sufficient

137 material were split for elemental analysis. Experimental particles were split after solvent extraction to

138 ensure removal of reactant polysulfide before S quantification.

139   All solvent-extracted particles were subjected to acid-volatile sulfide (AVS) extraction with hot

140   (~70°C) 6N hydrochloric acid under flowing N_2 (Rickard and Morse, 2005; Raven, Fike, Gomes, et al.,

141   2019). In addition to volatilizing sulfides from FeS, this method solubilizes a large proportion of the

142   carbohydrates and proteins in OM (Hill, 1965). After AVS hydrolysis, remaining solids were washed in

143   ultra-pure water and divided into splits for XAS and for elemental analysis.

144   *2.3 EA-IRMS analysis*

145   Carbon isotopes and S:N:C elemental ratios of lipid extracts and whole and AVS-extracted particles

146   were analyzed at UCSB with an Elementar Vario Isotope Select elemental analyzer (EA), which includes

147   a ramped-temperature column to improve SO_2 peak shape, coupled to a Nu Horizon isotope ratio mass

148   spectrometer (IRMS). C-isotope data were internally standardized to CO_2 gas standards and calibrated to

149   VPDB using the caffeine isotope standards USGS-61, -62, and -63. Reported uncertainties reflect long-

150   term uncertainties for replicate sulfanilamide standards. Whole particle samples before acidification retain

151   some seawater sulfate, as quantified by XAS (below); reported S:C ratios for OM were corrected to remove

152   contributions from inorganic phases (sulfate and FeS; Table S2). S-isotope values for dissolved sulfate at

153   the end of the polysulfide exposure experiment and for the initial polysulfide spike were measured by EA–

154   IRMS as barium sulfate and zinc sulfide, respectively. Samples contained WO_3 as a combustion aid, and

155   S-isotope values were calibrated to VCDT using the isotope standards IAEA-S1, S2, S3, and S5. The $\delta^{34}S$

156   values for the ^{34}S-labeled polysulfide spike are estimates because they exceed the calibration range of these

157   standards.

158   *XAS/XRF analysis and data processing*

159   The redox speciation and bonding environment of sulfur and iron in the particle filters were analyzed

160   at the Stanford Synchrotron Radiation Lightsource (SSRL). Glass fiber filter pieces were adhered onto Saint

161   Gobain M60 S-free polyester tape and covered in 5-μm-thick SPEX 3520 polypropylene XRF film. 'Bulk'

162   sulfur k-edge spectra (500 μm^2 spot size) were collected on beam line 14–3 on whole particles, solvent-

163   extracted particles, HCl-extracted particles, and lipid extracts, before and after copper exposure.

164   Additionally, a micro-focused X-ray beam was used to map S and Fe species by rastering over selected

165   mapping areas at specific energies (for sulfur: 2472.0, 2472.9, 2473.9, 2474.25, 2476.15, 2477.8, 2481.4,

166   2482.6, and 2486.0 eV; for iron: 7116.0, 7128.0, 7133.0, 7139.0, and 7147.0 eV) to create elemental and

167   chemical distribution maps. Full XAS spectra were collected from 2460 to 2540 eV (sulfur) or 6900 to 7500

168   eV (iron) at selected spots.

169   Sulfur data were collected at SSRL beam line 14–3, which is equipped with a Si(111) ($\Phi = 90$) double

170   crystal monochromator and calibrated to the thiol pre-edge peak of thiosulfate at 2472.02 eV. The S Kα

171   fluorescence line was measured with a Si Vortex Si drift detector (Hitachi) using Xspress3 pulse processing

172   electronics (Quantum Detectors). The X-ray beam was focused using an axially symmetric focusing mirror

173   (SIGRAY) to a size of 5 x 5 µm at a flux of ~8 x 10^{10} photons per second; maps were collected at a resolution

174   of 5 µm^2. Sulfur XAS spectra were processed in the SIXPACK (Webb, 2005) software package using a K-

175   edge E0 of 2473 and pre-edge and post-edge linear normalization ranges of –20 to –7 and 35 to 70 eV,

176   respectively. Uncertainties reported in Table S3 refer to the confidence in the linear combination fit

177   calculated in SIXPACK. Iron data were collected at SSRL beam line 2–3, a bending magnet workstation

178   equipped with a Si(111) ($\Phi = 0$) double crystal monochromator calibrated such that the first derivative of

179   an Fe metal foil was set to 7112 eV. The beam line uses an axially symmetric focusing mirror (SIGRAY)

180   to achieve a spot size of 5 x 5 µm at a flux of ~5 x 10^8 photons per second at 7100 eV, and uses a similar

181   fluorescence data collection system as above with 14-3 to collect k-edge Fe spectra from 6900 to 7500 eV

182   and elemental maps of Ca, P, Mn, Ti, S, and other metals at 5-µm resolution. XRF maps from both beam

183   lines were processed using the MicroAnalysis Toolkit (SMAK; (Webb et al., 2011)). Sulfur XANES fitting

184   used 3-pt blurred maps (standard deviation 0.5) and a set of six standard spectra (FeS, methionine,

185   glutathione disulfide, methionine sulfoxide, cysteic acid / sulfonate, and sulfate ester).

186

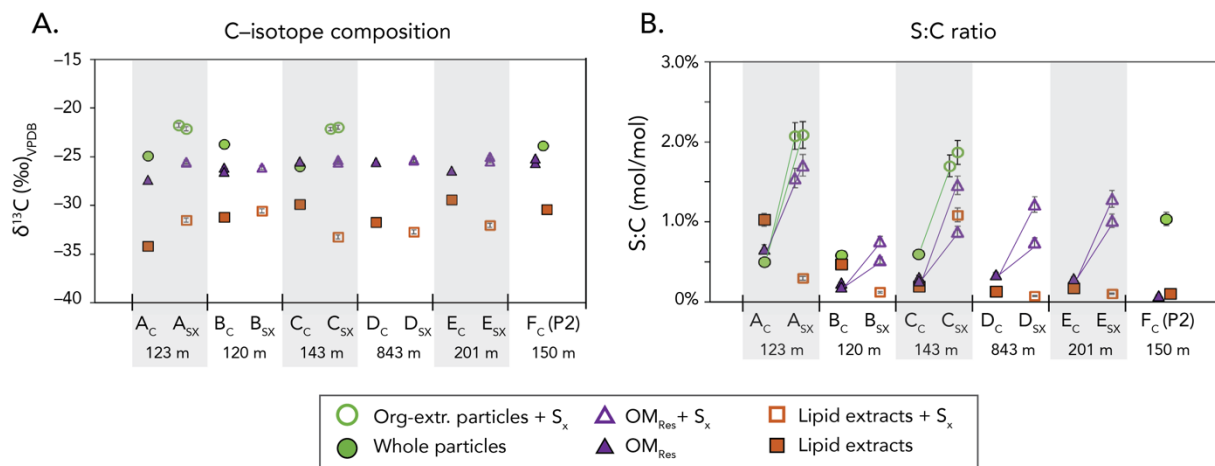187   **3. Results**

3.1 EA–IRMS results

Fig. 1: Carbon-isotope composition and molar S:C ratio of particle materials, before and after S_x exposure. S:C ratios exclude inorganic phases (sulfate and FeS) quantified by XAS; uncorrected ratios are reported in Table S2. Filled symbols represent controls (e.g., 'A_C'), and hollow symbols represent experiments (e.g., 'A_{SX}'), as detailed in Table S1. Whole and organic-solvent-extracted particles represent the combination of OM_{Hyd} and OM_{Res}. Samples with multiple symbols represent discrete filter splits rather than replicates of homogenized samples. Error bars indicate the long-term reproducibility of standards (2σ). In panel B, purple and green lines highlight the consistent increase in the S:C ratio of OM_{Res} and whole particle samples following sulfurization; bulk lipids do not show a consistent trend.

The carbon-isotope compositions of sinking particle materials are similar for samples from both the high- and low-particle-flux sites (A–E and F, respectively; Fig. 1A and Table S2). Whole washed particles before acidification, which may contain both organic C and calcium carbonate, have $\delta^{13}C$ values between –26.0 and –23.7‰ (mean –24.6‰), while lipid extracts have relatively ^{13}C-depleted compositions (Hayes, 2001) between –32.9 and –28.3‰ (mean –30.4‰). Accordingly, the $\delta^{13}C$ values for S_x-exposed, solvent-extracted particles are higher (mean –22.0‰) than those for whole particle controls due to the removal of ^{13}C-depleted lipids by solvent extraction (Fig. 1A). After both lipid extraction and strong

9

206   acidification (6N HCl, 70°C, 2 hrs), residual particle material (OM_{Res}) from both experiments and controls

207   has a $\delta^{13}C$ value between –27.4 and –25.0 (mean –25.7‰). There is no significant change in the C-isotope

208   composition of either OM_{Res} or OM_{Lipid} associated with S_x exposure.

209   The nitrogen contents of whole particles, lipids, and OM_{Res} primarily track the abundance of protein

210   in each pool (Fig. S1). Whole particles N:C ratios (8.9 – 15.3 mol%) are typical for protein-rich, primary

211   producer biomass that has experienced some degradation (16:117 = 13.7%; (L. Anderson and Sarmiento,

212   1994)), while lipid extracts have lower N:C ratios (0.6 – 3.8 mol%). Molar N:C ratios in OM_{Res} controls

213   are between 2.5 and 4.7 mol%. In some cases, S_x-exposed OM_{Res} contains significantly more N than OM_{Res}

214   controls, with N:C ratios of up to 7.8 mol% (sample D_{Sx}; Fig. S1).

215   Sulfur-isotope compositions of dissolved sulfate in experimental bottles are between 22.6‰ and

216   24.3‰, summarized in Table S2. Replicates of the polysulfide spike were trapped as zinc sulfide and thus

217   reflect thio sulfur (bisulfide and roughly half of polysulfide S); the effect of excluding zero-valent

218   polysulfide S is negligible in this case given the much larger uncertainties from standard extrapolation.

219   Spike $\delta^{34}S$ values average 342.2‰ (Table S3).

220   Particle S:C ratios (Fig. 1B) increase in response to S_x exposure, reflecting the addition of

221   (poly)sulfide S to particulate OM. In controls, the S:C ratio of organic materials in whole particles is 0.64–

222   0.74 mol% at high-flux site P1 and 1.3 mol% in one sample from low-flux site P2 (Table S2). OM_{Res} and

223   lipids have lower S:C ratios, averaging 0.3 mol% and 0.4 mol%, respectively. After sulfurization, organic

224   materials in whole and solvent-extracted particles from P1 have S:C ratios between 1.7 and 2.1 mol%, an

225   approximately 2.8-fold increase over P1 controls. Similarly, average S_x-exposed OM_{Res} S:C ratios average

226   1.1% (range 0.5 – 1.7%), a roughly 3.3-fold increase over P1 controls. Lipid extract S:C ratios are variable

227   among samples (0.1 – 1.1%) and do not differ systematically between controls and S_x-exposed samples.
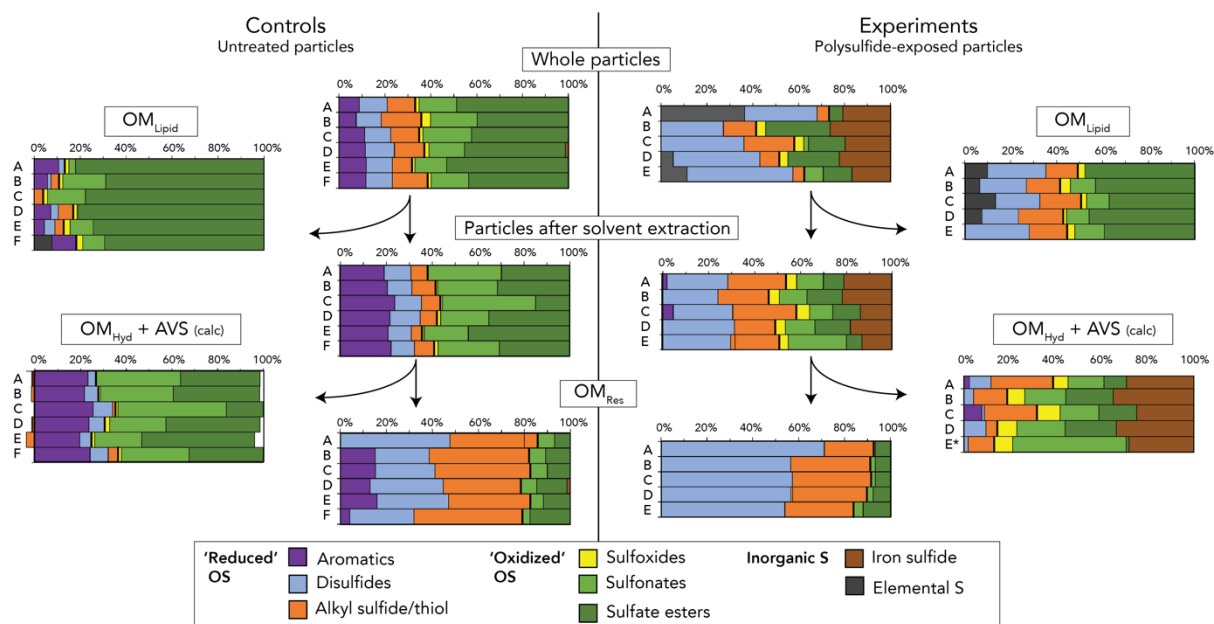
228

229   **3.2   Bulk Particle XAS Speciation**

Fig. 2   Sulfur speciation in sinking ETNP particles, with and without polysulfide exposure. Samples A through F represent six separate trap deployments (see Table S1). Heavy black lines between the orange and yellow bars broadly separate 'reduced' from 'oxidized' organic sulfur species. Inorganic sulfate was also detected in samples before hot acidification and is excluded from normalization. Non-sulfate materials lost during hot acidification are calculated by difference using x-ray spectrum step heights and are subject to errors of 5–10%. One sample labeled E* used an assigned step height. Fit uncertainties on each component are typically <2% (see Table S4). The elemental S detected in experimental whole particles (grey) may derive from polysulfide reactants; this was removed from lipid extracts before analysis by Cu exposure.

The redox speciation of sulfur in particles varies systematically among lipid, hydrolyzable, and hydrolysis-resistant materials, and these distributions are consistent across samples from both sites and all depths (Fig. 2). Broadly speaking, the OS in whole (control) particles from the ETNP is approximately 60% oxidized (sulfonates and sulfate esters) and 40% reduced (sulfides, disulfides, and aromatics). Organic solvent extracts are predominantly (58–78%) sulfate esters with up to 16% sulfonates, and the remaining

11

246   3.2 – 16.1% of the lipid OS pool is reduced. Hot acidification (6N HCl, 70°, 2 hrs) removed approximately

247   85% of the total sulfur in the particles, which included most of the non-lipid oxidized OS as sub-equal pools

248   of sulfate esters and sulfonates. A reduced OS component is also removed by acidification that is best fit as

249   aromatic S. After acidification, residual solids (OM_{Res}) contain sulfur predominantly as sulfides and

250   disulfides, with smaller amounts of aromatics and oxidized forms, as was previously reported for parallel

251   experiments with this population of particles (Raven et al., 2021).

252   After exposure to polysulfides for ~48 hrs, the speciation of sulfur in all five of the particle samples

253   from site P1 was transformed, as summarized on the right-hand side of Fig. 2. Compared to controls, S_x-

254   exposed particles contain a larger proportion of reduced species (sulfides and disulfides) and iron sulfides.

255   S_x-exposed whole particles contain some elemental sulfur derived from the polysulfide reactant solution

256   that was subsequently removed by solvent extraction and copper exposure. Copper-treated lipids after

257   polysulfide exposure contained nearly 50% reduced OS in addition to the sulfate esters and sulfonates

258   observed in the OM_{Lipid} controls. Reduced OS in the S_x-exposed lipids is composed of sulfides and

259   disulfides with some zero-valent S. Particle materials lost during acidification include iron sulfides (AVS)

260   and roughly sub-equal pools of reduced and oxidized OS (OM_{Hyd}). OS in OM_{Res}, on the other hand, is

261   almost exclusively reduced (sulfides and disulfides). Oxidized OS thus makes a smaller contribution to

262   total OS in the experimental particles than in corresponding controls.
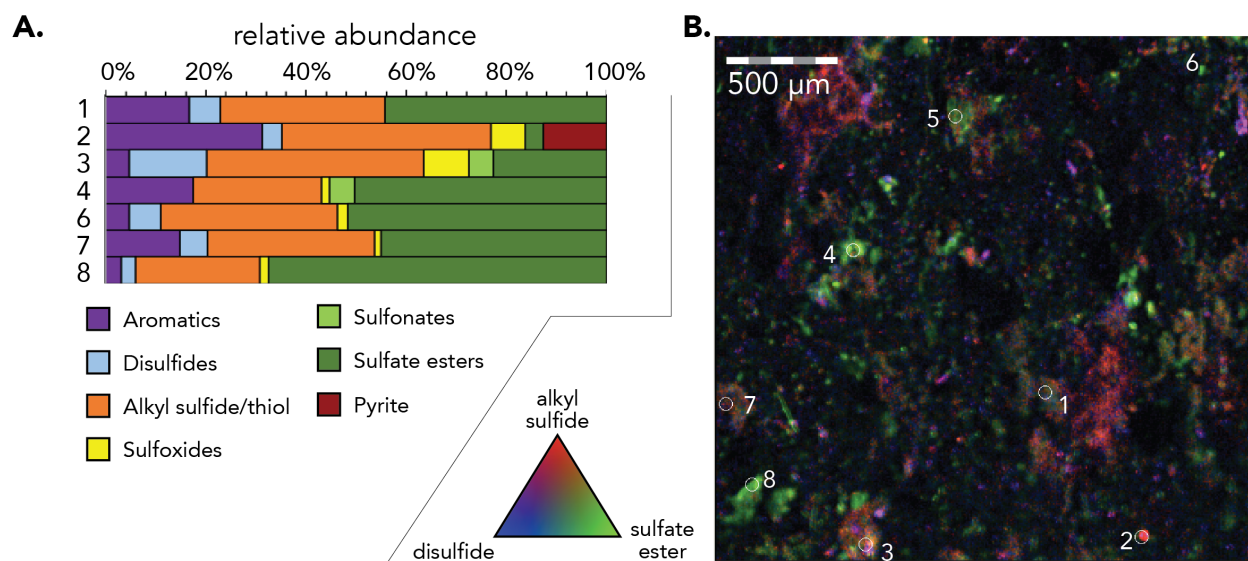
263

264   **3.3**   **Particle XRF Maps**

Fig. 3 Sulfur speciation of whole particle controls by XAS and XRF. Particles were collected from site P1 (123 m, sample 'A$_C$') and are mounted on GFF filters. Panel A: Fitted XAS spectra for specific (~1 μm^2) spots, numbered at right. Uncertainties are typically <2%, see Table S5. Panel B: Tri-color XANES fits to multiple-energy maps showing alkyl sulfides and thiols (red), disulfides (blue), and sulfate esters (green). Map step size = 7 μm.

To examine the spatial variability in particle OS speciation, we mapped particles at 5-to-7-μm resolution using x-ray fluorescence imaging. Figure 3 presents maps of sulfur speciation in whole, buffer-washed particles from site P1 at 123 m depth (sample 'A$_C$'). Organic sulfur speciation is spatially heterogeneous in control particles, with separate regions that are rich in reduced versus oxidized organic S. The abundance of reduced organic S as specific spots ranges from 20.5% (spot 8) to 72.5% (spot 2). Reduced organic S, including alkyl sulfides, thiols, aromatics, and disulfides, appears as localized concentrations ranging from ≤ 7 μm (single pixel) to nearly 80 μm in diameter. Oxidized components (sulfonates and sulfate esters) are also found in discrete regions up to several hundred microns in size.
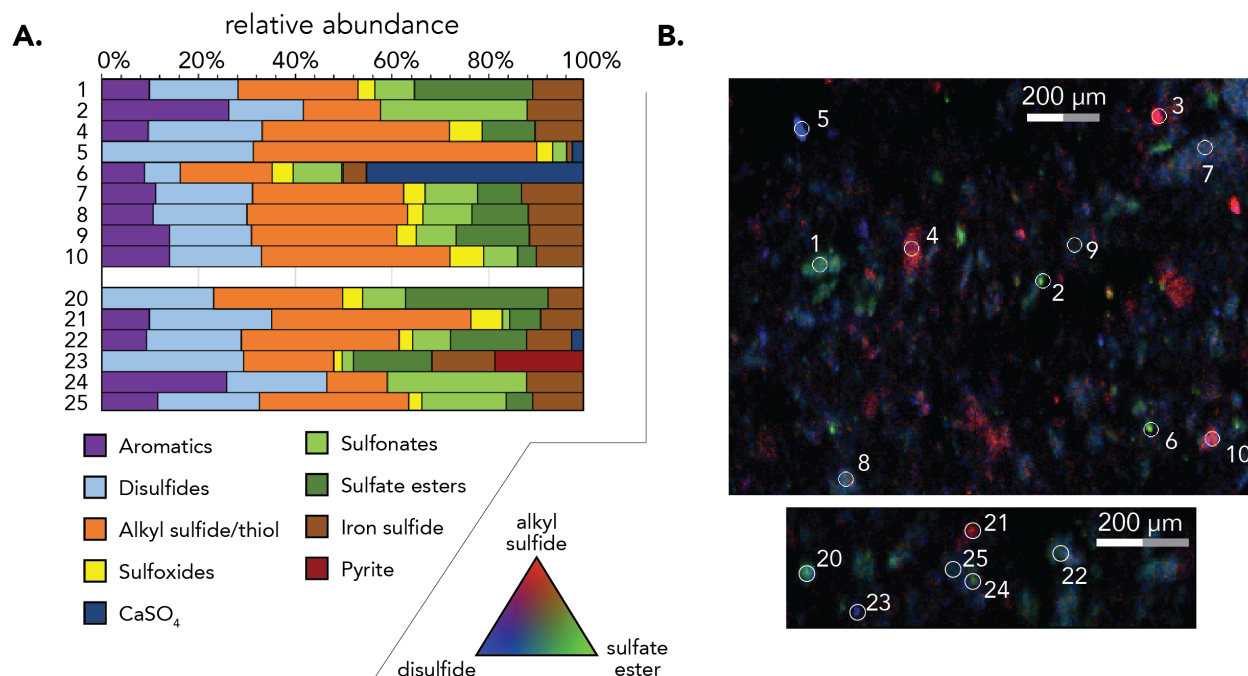
Fig. 4 Sulfur speciation maps of polysulfide–exposed particles by XAS and XRF. As in Fig. 3, particles were collected from site P1 (123 m, sample 'A$_{Sx}$') and are mounted on GFF filters. Panel A: Fitted XAS spectra for specific (~1 μm^2) spots, numbered at right. Uncertainties are typically <2%, see Table S5. Panel B: Tri-color XANES fits to multiple-energy maps from two adjacent filter regions, showing alkyl sulfides and thiols (red), disulfides (blue), and sulfate esters (green). Step size = 5 μm. Newly formed disulfides appear as diffuse, 50-to-100-μm regions surrounding more discrete particles containing various forms of organic S.

After exposure to polysulfides, particles accumulate alkyl sulfides and disulfides (Fig. 4). The proportion of OS in reduced forms (sulfides, disulfides, and aromatics) ranges from 59.3 to 78.3% (Fig. 4A and Table S5), and the overall proportion of reduced S is higher, consistent with the results for bulk speciation (Fig. 2). Newly formed disulfides appear as diffuse splotches that are generally but not exclusively associated with other forms of organic S, especially alkyl sulfides (e.g., spot 7). Regions that are relatively rich in oxidized OS are discrete and 100–200 μm in size, similar to those observed in controls.

14

295 In contrast, iron monosulfides are found throughout sulfurized particle materials and do not generally

296 accumulate as singular particulates. Despite its relatively low abundance, the presence of FeS in these

297 samples is confirmed by the characteristic pre-edge peak near 2470 eV in the XAS spectra from Fig. 4A.

298 Gypsum (calcium sulfate) was also detected as an individual 25-μm-diameter particulate (spot 6).
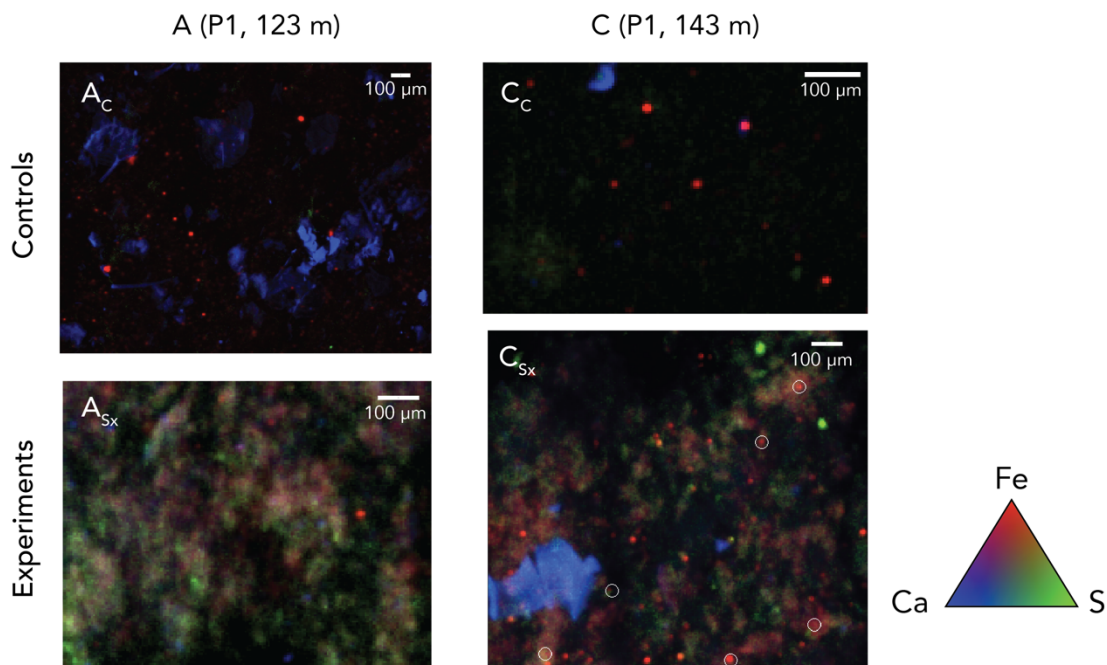
299

301 **Fig. 5: Maps of iron, calcium, and sulfur on particle filters by XRF.** Samples were prepared by washing

302 with buffer under anoxic conditions; sulfur maps in all panels thus include trace inorganic sulfate. Maps

303 show representative regions from sample splits, not the same regions after treatment. Pixels are 5 μm^2.

304 Colors show iron at 7133 eV (red), total calcium (blue), and total sulfur (green).

305 Most of the iron on the particle filters is present as discrete, 15–40 μm particulates (Fig. 5). Prior

306 to polysulfide exposure, iron oxyhydroxides are scattered throughout the samples and are not spatially

307 associated with either carbonates or organic matter (P or S). After polysulfide exposure, some of these

308 discrete iron particulates remain (e.g., C_{Sx}, Fig. 5), but iron also accumulates throughout the particles as a

309   diffuse phase that is broadly co-located with sulfur. Based on XAS spectra in Fig. 4, at least some of this

310   material is FeS (e.g., mackinawite).

311

312   **4.   Discussion**

313   *4.1   Controls: Organic sulfur speciation in sinking marine particles*

314   Sulfur is a major component of biomass: molar S:C ratios for marine biomass are typically 0.5–

315   1‰, although they can be lower in woody plants and higher in some S-cycling microorganisms (Matrai and

316   Eppley, 1989; Chen et al., 1996). The speciation of organic sulfur in particles (Fig. 2) reflects the

317   contributions of various compound classes to functionally defined categories of OM, as well as any

318   subsequent transformations of that OM due to enzymatic degradation, condensation, oxidation, and/or

319   sulfurization.

320   Sinking particles from the ETNP ODZ contain the full suite of reduced and oxidized OS moieties

321   that have been previously described for proteins, lipids, and carbohydrates. A large proportion (42–65%)

322   of the assimilatory S in microplankton is typically found as proteins and polypeptides (Cuhel et al., 1982),

323   specifically the amino acids cysteine, which is a thiol, and methionine, which is an alkyl sulfide. Cysteine

324   and methionine are highly susceptible to oxidation, both in the environment and during laboratory handling,

325   which will produce sulfoxide (Vogt, 1995) and/or sulfonate (Phillips et al., 2021). The AVS hydrolysis

326   method used here to isolate OM_{Res} is shorter in duration but otherwise similar to some early methods for

327   protein hydrolysis (e.g., 24 hrs, 110°, 6N HCl) (Hill, 1965), although this method can leave behind some

328   especially hydrophobic linkages in OM_{Res}, like methionine. Therefore, AVS hydrolysis is likely to

329   solubilize many proteins in our particles, which is supported by the drop in molar N:C ratios from whole

330   particles (averaging 11.6%) to OM_{Res} (averaging 4.5%; Fig. S1). However, we find that most of the OS in

331   the OM_{Hyd} pool is relatively oxidized (Fig. 2), suggesting that cysteine and methionine are not major

332   contributors to OM_{Hyd}. (We calculate speciation by comparing solids before and after hydrolysis, so the

333   lack of reduced S in OM_{Hyd} is not caused by amino acid oxidation during hydrolysis.) Instead, the reduced

334   OS species in OM_{Hyd} are best fit as aromatic, and the main peak in their XAS spectra at ~2473.5 eV is

335   resolvably shifted relative to cysteine and methionine. Aromatic OS compounds have been seen to form

336   rapidly (i.e., phytol thiophene, (LaLonde et al., 1987; Raven, Sessions, Adkins, et al., 2016)), but the

337   immediate provenance of apparently aromatic OS in OM_{Hyd} is not yet known. Rather than appearing in

338   OM_{Hyd}, sulfides account for ~80% of the S in OM_{Res} from control particles, and they are localized in cell-

339   sized (≤ 20 um) structures that suggest these sulfides may be proteinaceous (Raven et al., 2021). In addition

340   to the thiols and alkyl sulfides in amino acids, these discrete, sulfide-rich structures contain disulfides that

341   may reflect amino acid dimers, like cystine, and other sulfides could reflect low-molecular-weight thiols

342   like the common antioxidant glutathione (Matrai and Vetter, 1988). Finally, even in these unamended

343   'control' samples, we expect to have at least trace contributions of sulfides and/or disulfides to OM_{Res} from

344   *in-situ* OM sulfurization, as we observed using radiolabels in Raven et al. (2021).

345   Oxidized OS compounds comprise the majority of total OS in lipids, OM_{Hyd}, and whole particles.

346   Major known categories of sulfur-bearing lipids include sulfonium compounds like sulfoquinovosyl

347   diacylglycerides (SQDGs; corresponds to 'sulfonate' in our XAS categorization) and sulfate-ester-bearing

348   compounds like sulfogalactosylglycerolipid (SGG), sulfated hormones (e.g., cholesterol sulfate), and other

349   sulfoglycolipids common in animals (Benson et al., 1959; R. Anderson et al., 1978; Ishizuka, 1997). In our

350   samples, lipid S is rich in sulfate esters, which represent 41–50% of lipid OS at site P1 and 34% at site P2.

351   Higher relative abundances of sulfate esters at site P1 are generally associated with higher S:C ratios (up to

352   1.0%), while lipids from P2 have a S:C ratio of 0.1%. Lipid sulfonates represent a relatively minor

353   contribution to lipid extracts (up to 15.8 ±1.4%).

354   Carbohydrates appear to be major sources of the OS in OM_{Hyd}, and this apparent carbohydrate OS

355   is primarily composed of sulfate esters (Fig. 2). Exudates from macrophytoplankton can be major sources

356   of sulfate-ester-bearing polysaccharides (Ramus and Groves, 1974; Percival et al., 1980) and are likely to

357   be particularly important here, because these extracellular polysaccharides, which can be produced in vast

358 quantities by diatoms, are thought to contribute directly to the formation of large, sinking particles

359 (Alldredge and Silver, 1988; La Rocha and Passow, 2007; Arnosti et al., 2021; Vidal-Melgosa et al., 2021).

360 Hydrolyzable sulfate esters are also frequently localized in irregularly sized particles (Fig. 3) that could

361 represent detritus from plants and animals and/or sulfated polysaccharides from algal exudates (Vidal-

362 Melgosa et al., 2021). Overall, these XAS data underscore the substantial contributions of oxidized OS

363 species to lipids and carbohydrates in marine particles, which can be clearly distinguished from amino acids

364 and the products of abiotic OM sulfurization.

365

366 *4.2   Experiments: Organic products of particle sulfurization reactions*

367   In a separate study using this same population of particles (Raven et al., 2021), we added

368 radiolabeled sulfate to concentrated particle incubations in order to estimate rates of microbial sulfate

369 reduction, and we identified organic S formation under anoxic, sulfide-limited, ODZ-like conditions. In

370 those experiments we were not able to identify the speciation of small quantities of sulfurization products

371 against a background of abundant OS in biomass. Here, we expose particles to seawater containing 0.5 mM

372 polysulfides for two days to evaluate their sulfurization potential under sulfidic conditions, which also

373 allows us to clearly resolve the speciation of newly formed abiogenic OS. These polysulfide concentrations

374 are equivalent to or slightly higher than reported concentrations in a range of modern environments: the

375 Great Salt Marsh (Boulegue et al., 1982; Luther et al., 1986), sulfidic lakes like Mahoney Lake (Overmann

376 et al., 1996) and Fayetteville Green Lake (Zerkle et al., 2010), and the Black Sea (Holmkvist et al., 2011).

377 Polysulfide concentrations can be even higher in specific environments like microbial mats, where up to

378 100s of mM polysulfides have been reported (Findlay, 2016). Conditions in experimental bottles therefore

379 coarsely reproduce the experience of particles in certain modern and ancient Earth environments.
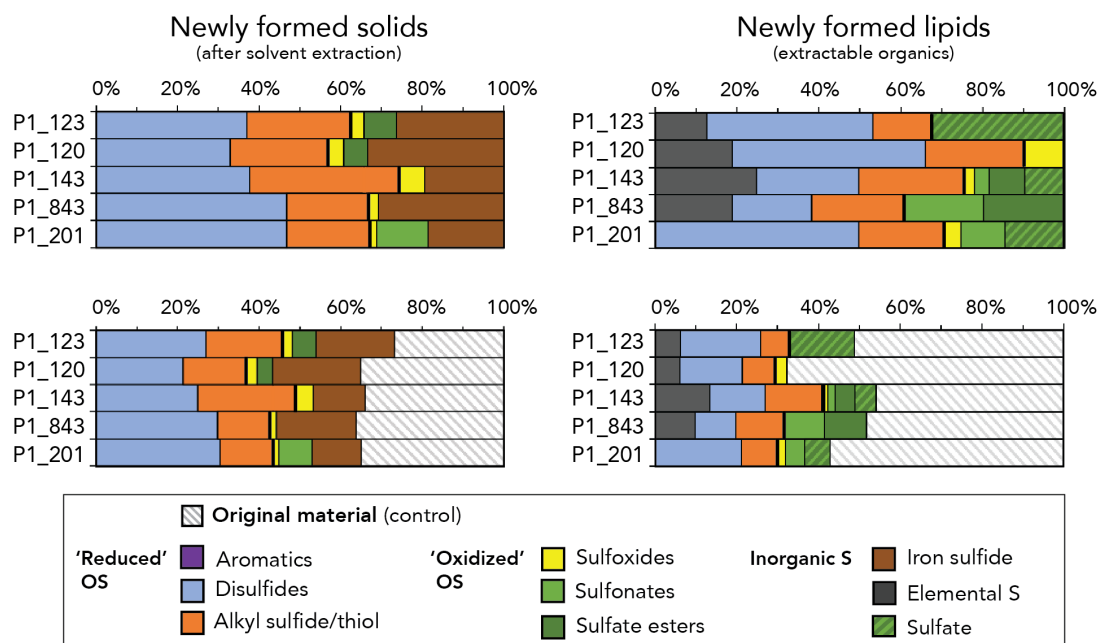
Fig. 6 Speciation of products formed during polysulfide exposure. Heavy black lines broadly separate 'reduced' from 'oxidized' organic sulfur species. Results were calculated by linear combination fitting of S_x-exposed sample spectra for solvent-extracted particles (OM_{Res} + OM_{Hyd}, left) and lipid extracts (right) using the control spectra from each sample as a component. Upper and lower panels show the same data, but the lower panel highlights the proportion of S_x-exposed materials that were attributed to pre-existing (control) materials. Newly formed organic S in both pools is largely sulfides and disulfides.

Experiments with particles and (poly)sulfide generated organic S in the proto-kerogen, hydrolysable, and lipid pools. Based on XAS fits, organic S accounts for between 67 and 82% of the newly formed non-lipid particle solids (Fig. 6); inorganic products (iron sulfides) are discussed in Section 4.3, below. The initial molar S:C ratios in total particle OM from high-flux site P1 average 0.69% (range 0.64 – 0.74%), and these ratios increase after 48 hours of polysulfide exposure to an average of 1.9% (range 1.7 – 2.1%). OM S:C ratios are somewhat lower in the OM_{Res} pool, averaging 0.33% before, and 1.1% after, polysulfide exposure (Fig. 1B). These S:C ratios are similar to those found in OM_{Res} in sediments from O_2-limited continental margin sediments, including the Santa Barbara Basin (OM S:C ratios average 2.1 mol%

396   in the upper 50 cm; (Raven, Sessions, Fischer, et al., 2016)), the Peru Margin (0.5 – 2.3% in the upper meter

397   of sediments; (Mossman et al., 1991; Suits and Arthur, 2000), and the Namibian Margin (OM S:C ratios

398   average 2.3% for all data; (Dale et al., 2009)). But, sulfurized particle S:C ratios remain below those

399   observed for OM in sulfidic basins like the Cariaco Basin (~4 mol%; (Werne et al., 2003)). It is likely that

400   longer–term exposure to polysulfides would further increase the S content of particle OM, eventually

401   reaching 'saturation' or full sulfurization of the functional groups that are reactive on the timescale of

402   interest, as modified by other environmental factors (Amrani et al., 2007). The change in particle S:C ratios

403   as a result of sulfurization indicates that organic precursor molecules contained at least that density of

404   rapidly sulfurizable functional groups (aldehydes, ketones, certain re-arrangable alcohols, and conjugated

405   double bonds (Kutuzov et al., 2019)).

406   The short duration of these 48–hour experiments makes it possible to investigate potential OM

407   preservation processes on the same timescale as particle OM breakdown and remineralization. Typical

408   sinking particle OM remineralization rates are ~12% per day (Iversen and Ploug, 2013; Cavan et al., 2017),

409   which means that reactions that transform particle OM within days are particularly important for impacting

410   the extent of OM remineralization in sinking particles and, by extension, carbon fluxes to the sediments.

411   Additionally, the large changes in organic S chemistry observed within 48 hours in these experiments

412   demonstrate that even intermittently sulfidic conditions – on the timescale of hours to days – can have a

413   dramatic effect on the composition of particulate OM.

414   The initial products of particle sulfurization are primarily organic sulfides and disulfides (Fig. 6).

415   Although three of the five sulfurized samples also contained more sulfonates or sulfate esters than their

416   respective controls, this likely represents heterogeneity in the distribution of assimilatory OS particles

417   among control and experiment filter aliquots. In Figure 6, the speciation of newly formed materials is

418   calculated by assuming that sulfurization adds new sulfur to an unchanging pool of biogenic OS, as

419   measured in the control sample. The calculated, newly formed OS is very similar to the overall speciation

420   of S_x-exposed OM_{Res} (Fig. 2) and is consistent with observations from the sulfurization of standard

421   compounds under conditions similar to those investigated here (Amrani and Aizenshtat, 2004b). In those

422   experiments, α, β-unsaturated aldehydes, including the chlorophyll-derived C_{20} isoprenoid phytenal, were

423   exposed to a polysulfide solution and the products were identified as disulfide-bridged oligo-polymers.

424   Nucleophilic polysulfides attacked the conjugated double bond rapidly (within hours) and the carbonyl

425   group more slowly, leading to carbon skeletons cross-linked by two or more S_x (e.g., disulfide) bridges

426   within days to weeks (Amrani and Aizenshtat, 2004b). Similar mechanisms could explain the observed

427   rapid formation of organic sulfides, disulfides, and polysulfides ($S_{x\geq 3}$) during the sulfurization of sinking

428   marine particles.

429   Reports of the experimental sulfurization of dissolved OM (1 hr, 20°C, artificial seawater) that used

430   selective degradation experiments and high-resolution molecular analysis described generally more

431   oxidized S moieties, especially sulfonates, than we see for sinking particles (Pohlabeln et al., 2017). The

432   lack of abiogenic sulfonates in our particulate sulfurization experiments (Fig. 6) thus suggests that distinct

433   OM sulfurization pathways exist for different OM pools in the marine environment and by extension that

434   OS speciation could be a valuable indicator of the OM sources experiencing sulfurization.

435   One possible reason for the existence of different OM sulfurization pathways is the diversity of

436   organic precursors involved. Even within the pool of particulate OM in sinking marine particles, potentially

437   sulfurizable precursors include cells, fecal pellets, detritus, and extracellular polymers (Alldredge and

438   Silver, 1988). In Fig. 4, organic disulfides appear within certain particle regions that range from 30 to 300

439   μm in diameter. These 'strongly sulfurized' regions often envelop clusters of small (single-pixel; ≤ 5 μm),

440   sulfide-rich particulates that are interpreted as cells. And, they are also frequently associated with the larger

441   (20–200 μm), sulfate-ester-rich irregular particles that may represent concentrations of polysaccharide

442   exudates or contributions from plant or animal detritus. These spatial relationships suggest that sulfurization

443   affects a ubiquitous particle component that naturally contains a lower concentration of organic S than other

444   forms of biomass. Exopolymeric substances (EPS) are a leading candidate for this component. EPS is a

445   loosely-defined blend of polysaccharides, proteins, nucleic acids, and lipids, with carboxylate, amine,

446   hydroxyl, sulfate, and phosphate functional groups (Alvarado Quiroz et al., 2006; Braissant et al., 2007).

447   EPS is an important contributor to the formation of large, sinking particles, building particle size and density

448   by binding organic and inorganic solid materials together (Alldredge and Silver, 1988; Passow et al., 1994;

449   Bhaskar and Bhosle, 2005). The abundance of EPS in large sinking particles may make these organic

450   materials particularly susceptible to rapid sulfurization.

451   XAS results strongly indicate that lipids sulfurize alongside non-lipid OM over 48 hours of

452   polysulfide exposure, despite the lack of consistent trends in lipid S:C ratios. Newly formed lipid OS is

453   compositionally similar to newly formed non-lipid OS, with varying proportions of sulfides, disulfides, and

454   oxidized species. Sulfurized lipids also contain zero-valent S that may represent the S^0 atoms in S_3 and

455   longer organic polysulfides that remained despite exposure to activated copper. Longer ($n \geq 3$) polysulfide

456   bridges may therefore be more important in lipids than for other organic precursors (Fig. 6). Rapid lipid

457   sulfurization has been documented for specific molecules both experimentally and in the environment (Van

458   Mooy et al., 2002; Amrani and Aizenshtat, 2004b; Raven, Sessions, Adkins, et al., 2016), while some lipids

459   are also known to sulfurize over thousands of years under sulfidic conditions (Kok, Rijpstra, et al., 2000;

460   Werne et al., 2000). However, the data presented here represent some of the first results to address lipids

461   as a bulk pool and to evaluate the quantitative significance of rapid sulfurization to this pool overall.

462   Inconsistent trends in lipid S:C ratios following sulfurization may reflect changes in the

463   extractability of lipids caused by sulfurization reactions and/or the heterogeneous distributions of specific

464   particle components that are key sources of sulfated lipids. In the first case, the higher molecular weight

465   oligo-polymers produced by lipid sulfurization products would be generally expected to be less soluble than

466   their monomers; in prior phytenal sulfurization experiments, sulfurized lipid products visibly precipitated

467   from solution (Amrani and Aizenshtat, 2004b). Still, any lipids added to OM_{Res} due to sulfurization were

468   insufficient to significantly lower the C-isotope composition of OM_{Res} (Fig. 1A). Alternatively, the

469   relatively large sample-to-sample variation among lipid extract S:C ratios and the inconsistent trends in

470   response to sulfurization may both reflect the heterogeneous distribution of relatively small numbers of

471   specific particle types with very different concentrations of sulfate ester-bearing lipids. Many sulfatides

472   and/or hormone conjugates like cholesterol sulfate are produced in large quantities by certain animals

473   (Metzger et al., 1995), and small fragments of such detritus could be localized sources of S-rich lipids in

474   specific filter aliquots (Ishizuka, 1997).

475

476   *4.3   Experiments: Competitive sinks for polysulfides*

477   Sulfide has many possible reaction pathways in real, complex marine particles. In addition to

478   reactions with OM, both microbial sulfide oxidation and iron sulfidization can occur rapidly, generating

479   inorganic sulfur species with redox states ranging from S^0 to sulfate, and iron sulfides, respectively.

480   We use the appearance of ^{34}S-labeled sulfate to estimate the scale of polysulfide oxidation during

481   the 48-hour experiment. The $\delta^{34}S$ value of seawater sulfate increased during the experiment to values

482   between 22.6 ± 0.4‰ and 24.3 ± 0.4‰, a significant change from initial sulfate at ~21‰. Given a 28 mM

483   concentration of seawater sulfate, these values indicate the addition of between 140 and 295 μM sulfate

484   with a $\delta^{34}S$ value matching the polysulfide spike (~342‰), which represents a substantial proportion (27 –

485   57%) of the 520 μM polysulfide solution originally added to each experiment. Some of this (poly)sulfide

486   oxidation may have occurred abiotically through reaction with any dissolved O_2 that was introduced during

487   on-deck handling of these 'net wash' samples and incompletely removed during gentle sparging with N_2.

488   However, even dissolved O_2 concentrations of as much as 10 μM would account for only a few percent (~5

489   μM) of this sulfate production. A larger amount of (poly)sulfide oxidation likely occurred through microbial

490   processes. Microbial sulfide oxidation can be highly efficient at drawing down limiting sulfide

491   concentrations, generating a tightly coupled and often cryptic sulfur cycle in sediments (Canfield et al.,

492   1992; Jorgensen, 2019) and the water column (Canfield et al., 2010; Johnston et al., 2014). However, sulfide

493   oxidation in the dark still requires an oxidant like O_2 or metal oxides. Alternatively, some microorganisms

494   can directly metabolize polysulfides, including by disproportionation, which does not require an external

495   oxidant (Findlay, 2016). Multiple pathways of sulfide oxidation and polysulfide metabolisms likely

496   contributed to the net (poly)sulfide oxidation rates observed in our experimental bottles, which, at ~100

497   μM/day, are similar to sulfide oxidation rates reported for very different environments like shallow marine

498   sediments (Findlay et al., 2020). For our purposes, microbial (poly)sulfide oxidation is a major sink for

499   polysulfide reactants in the presence of marine particles, and it reduced the total amount of sulfur reactant

500   for other reactions by 27 to 57%. OM sulfurization occurs in particles despite this active competition for

501   (poly)sulfide from oxidative sinks. Although this oxidative cycle likely generated some quantity of more

502   oxidized inorganic sulfur species (e.g. thiosulfate), the key reactant for OM sulfurization is still most likely

503   polysulfide because this matches the redox state of the newly formed organic S.

504   Another important sink for (poly)sulfide in particles is the formation of iron sulfides. The initial

505   product of the reaction between Fe^{2+} and S^{2-} is an iron monosulfide (e.g., FeS(aq), mackinawite). Given

506   unlimiting sulfide, the rate of this reaction depends on the availability of Fe^{2+}, which is typically sourced

507   from the reduction of Fe(III)-oxyhydroxides and other reactive Fe(III) species. Poorly crystalline

508   oxyhydroxides react at rates that are several orders of magnitude higher than the rates of reaction for Fe-

509   bearing silicates (Canfield et al., 1992). However, these model iron compounds may not always be

510   representative of the active species in the marine iron cycle (Resing et al., 2015). For example, marine

511   particles from ODZs are rich in sorbed Fe^{3+} as iron oxyhydroxides (FeOOH), and this iron appears to be

512   actively recycled within ODZs between dissolved Fe^{2+} and particulate Fe(III) minerals (Heller et al., 2017).

513   We observe similar iron species in our control particle samples; the first-derivative x-ray spectra for iron in

514   these particulates (Fig. 5) are a good match for FeOOH (ferrihydrite). Before S_x exposure, these iron

515   oxyhydroxides are found in discrete, 10–50 μm-diameter particles with a broadly round morphology. These

516   iron-bearing particulates are found throughout the mapped samples (A, B, and C) and are not spatially

517   associated with calcium, phosphorus, or total sulfur.

518   Iron sulfides form within 48 hours of exposure to polysulfides. Unlike Fe(III) species, which were

519   present in discrete particles, FeS products accumulate in a diffuse manner throughout the samples (Fig. 5);

24

520   ratios of FeS to OS vary relatively little among all 24 spots in Fig. 4. Therefore, Fe(III) particulates do not

521   appear to be local FeS formation hotspots. Still, Fe(III) particulates must be the source of iron for FeS

522   formation because dissolved Fe^{2+} concentrations in the ETNP ODZ are only ~2 nM (*Bolster et al., under*

523   *review GCA*) and iron backgrounds in the EPS from controls are low (Fig. 5). FeS formation most likely

524   proceeds through the reductive dissolution of Fe(III) oxyhydroxides by sulfide to dissolved Fe^{2+}, which is

525   subsequently precipitated from solution as FeS. Iron-cycling microbes may also play a role in the generation

526   of dissolved Fe^{2+}. In either case, the exposure of discrete iron oxyhydroxide solids to polysulfides generates

527   diffuse, disseminated, small (sub-pixel; ≤5 μm) FeS particulates that are spatially associated with abiogenic

528   OS. Although greater temporal resolution is needed to evaluate the kinetic competition between sulfurizable

529   organic moieties and Fe^{2+} for sulfide, the concurrent and co-located formation of FeS and OS within 48 hrs

530   illustrates the tightly coupled formation of both inorganic and organic sulfur phases in sedimentary systems.

531   Sulfide-derived organic S accumulates before FeOOH consumption goes to completion, as seen in

532   Fig. 5. Similar observations have been made across diverse marine and lacustrine environments (Francois,

533   1987; Hartgers et al., 1997; Urban et al., 1999; Filley et al., 2002; van Dongen et al., 2003; Dale et al., 2009;

534   Raven, Sessions, Fischer, et al., 2016). These results demonstrate that organic matter and iron minerals can

535   be competitive sinks for (poly)sulfide over short (day) timescales, and that both organic and inorganic

536   sedimentary S phases may sample the same pool of (poly)sulfide reactant. The relative rates of formation

537   for organic and inorganic S are complex and will depend on the identities and morphologies of organic and

538   inorganic precursors, local geochemical conditions, and spatial relationships between sulfide sources and

539   potential sinks.

540

541   *4.4   Implications for the long-term preservation of sulfurized OM*

542   Because particle OM can sulfurize rapidly, even brief periods of sulfidic conditions in the

543   environment have the potential to transform the chemical structure of sinking particulate OM and impact

544   its lability. OM sulfurization is thus capable of transforming OM in temporally dynamic systems with only

545   intermittently sulfidic conditions, ranging from tidally and photosynthetically cyclic systems like microbial

546   mats and inter-tidal habitats to environments with strong seasonal upwelling. In sulfidic lakes and basins,

547   sinking particles that encounter a layer of polysulfide-rich water near the O_2–H_2S chemocline (Overmann

548   et al., 1996; Li et al., 2008) are likely to carry a signal of rapid OM sulfurization reactions to underlying

549   sediments, similar to interpretations of pyrite $\delta^{34}S$ values from the Black Sea and Cariaco Basin (Lyons,

550   1997; Lyons et al., 2003). The isotopic composition and speciation of organic sulfur preserved in sediments

551   will in part reflect rapid reactions in polysulfide-rich hotspots.

552   Prior to long-term burial, however, the initial products of particle sulfurization may experience

553   additional condensation reactions, enzymatic attack, and changing environmental conditions that could

554   further alter their chemistry. Subsequent alteration of metastable organic and FeS phases will potentially

555   impact sedimentary records of speciation and $\delta^{34}S$ values. Di- and poly-sulfides may be particularly

556   susceptible to isotope exchange and chemical maturation (Canfield et al., 1998), which would decrease the

557   proportion of organic polysulfides and disulfides over time and increase the abundance of monosulfidic or

558   aromatic moieties (Kohnen et al., 1991). Here, experimentally sulfurized OM was exposed to a solution

559   that was initially 50% polysulfides, which is expected to strongly favor the formation of organic di- and

560   poly-sulfides relative to reactions with sulfide (Kohnen et al., 1989). As a result, OM contains an average

561   of 52.4% disulfides (range 46.8 to 67.4%; Fig. 6, excluding FeS), which is significantly higher than control

562   OM_{Res} from untreated particles, which averages 31.3% (range 23.4 to 47.7%) disulfides, or than kerogens

563   from 100-million-year-old black shales, which have a maximum reported disulfide content of ~28%

564   (Raven, Fike, Bradley, et al., 2019; Raven et al., 2021). The zero-valent S atoms that are characteristic of

565   polysulfides were not apparent in OM_{Res} or OM_{Hyd}, but they were identified in sulfurized lipid extracts (up

566   to ~13% of newly formed lipid S). Regardless of chain length, the fate of these early-formed S–S bonds

567   during initial sediment diagenesis remains largely unknown. It has been suggested that organic polysulfides

568   exchange S-isotopes with dissolved, inorganic (poly)sulfides (Canfield et al., 1998), which could help

569   explain puzzling S-isotope distributions among sedimentary phases in shallow anoxic sediments (i.e., (Dale

570 et al., 2009; Raven, Sessions, Fischer, et al., 2016)). Rearrangement and maturation reactions could

571 potentially convert some disulfide moieties into the alkyl sulfides that are more common in ancient deposits.

572 Organic polysulfide maturation could also serve as a source of sulfur to other sedimentary reactions,

573 including the conversion of iron monosulfides to pyrite, S^0 disproportionation, or gradual lipid sulfurization.

574

575 **5. Conclusions**

576 The organic matter in sinking marine particles sulfurizes within 48 hours of exposure to

577 environmentally relevant concentrations (~0.5 mM) of polysulfides. The products of sulfurization are

578 primarily alkyl sulfides and disulfides, and they accumulate within regions of particles that are suggestive

579 of extracellular polymeric substances (EPS). This brief sulfurization roughly triples the sulfur-to-carbon

580 ratios of both bulk particles and hydrolysis-resistant OM_{Res}.

581 Lipids also sulfurize within 48 hours of polysulfide exposure, although less extensively than

582 apparent EPS or OM_{Res}. Sulfurized lipid products are also primarily alkyl sulfides and disulfides.

583 Iron monosulfide minerals form concurrently with organic S, which demonstrates that OM

584 sulfurization can occur on similar timescales to the reductive dissolution of FeOOH by (poly)sulfide. Iron

585 monosulfide products accumulate within diffuse regions of particles and appear together with OS products,

586 indicating formation via dissolved Fe^{2+}. Iron sulfides and organic S can form at the same time from a single

587 reactant pool, and the relative timing of their formation will depend on the availability and speciation of

588 iron and organic reactants.

589 Primary biogenic organic S in sinking marine particles from the ETNP ODZ is largely oxidized

590 and apparently composed of sulfated and sulfonated polysaccharides. Organic S in lipid extracts is primarily

591 in the form of sulfate esters, while hydrolysis-resistant OM_{Res} is composed of sulfides and disulfides.

592 Sulfides are concentrated within ≤ 7-to-80 μm-diameter particles that resemble cells or small fecal pellets

593 and appear to largely reflect amino acids. Sulfate esters are found in discrete, apparently hydrolysable

594   particles up to 200 μm across that may represent animal detritus or concentrations of sulfated

595   polysaccharides.

596   EPS appears to both sulfurize rapidly and potentially template the formation of iron monosulfides.

597   EPS, which plays a critical role in the formation of large marine particles, could make large, sinking

598   particles particularly susceptible to sulfurization. Additionally, subsequent transformations of sulfurized

599   OM during sedimentation and early diagenesis could further transform the speciation and/or isotopic

600   composition of organic S. For example, maturation and rearrangement of (poly)sulfide bridges could

601   transform some disulfides into monosulfides and bring the bulk speciation of S_x-exposed OM_{Res} closer to

602   that of ancient shales.

603   OM-rich particles that encounter polysulfides in the environment should be generally expected to

604   sulfurize and to accumulate organic sulfides and disulfides. This process has substantial implications for

605   the carbon cycle, both in response to anthropogenic climate change and during periods of Earth history with

606   relatively widespread sulfidic conditions. In the modern ocean, sinking particle sulfurization could help

607   explain the observation that sediments below a water column ODZ can have higher carbon contents than

608   those under water columns without a strong O_2 minimum, even when bottom water is oxygenated (Lückge

609   et al., 1996; Devol and Hartnett, 2001; B. Van Mooy et al., 2002; Keil et al., 2016). Due to the potential for

610   rapid OM sulfurization in the water column, the ongoing expansion of ODZs (Schmidtko et al., 2017) may

611   increase OM burial in even deep-water, O_2-exposed sediments. OM burial during Ocean Anoxic Event 2

612   (~94 Mya) was also likely enhanced due to water column particle sulfurization, drawing down atmospheric

613   CO_2 and impacting climate (Sinninghe Damsté and Köster, 1998; Hülse et al., 2019; Raven, Fike, Bradley,

614   et al., 2019). On even longer timescales, there is widespread evidence for locally sulfidic conditions at

615   intermediate water depths throughout the Proterozoic (Lyons et al., 2014; van de Velde et al., 2020). OM

616   sulfurization may have influenced the efficiency of carbon burial throughout this period, modifying the

617   organic carbon burial processes that contributed to the oxygenation of the surface Earth. On all of these

618   timescales, particle OM sulfurization in the water column is a powerful lever connecting changes in local

619 redox state to substantial transformations in the pool of OM delivered to, and preserved in, marine

620 sediments.

621

635

636 **Open Research / Data Availability**

637 All of the processed data used in this manuscript are presented in the main text and supporting information.

638 Data files are also archived on FigShare (*published upon manuscript acceptance*).

639

640   **<u>References</u>**

641   Alldredge A. L. and Silver M. W. (1988) Characteristics, dynamics and significance of marine snow.
642   *Progress in Oceanography* **20**, 41–82.

643   Alvarado Quiroz N. G., Hung C.-C. and Santschi P. H. (2006) Binding of thorium(IV) to carboxylate,
644   phosphate and sulfate functional groups from marine exopolymeric substances (EPS). *Marine*
645   *Chemistry* **100**, 337–353.

646   Amrani A. and Aizenshtat Z. (2004a) Mechanisms of sulfur introduction chemically controlled: δ34S
647   imprint. *Organic Geochemistry* **35**, 1319–1336.

648   Amrani A. and Aizenshtat Z. (2004b) Reaction of polysulfide anions with α, β unsaturated isoprenoid
649   aldehydes in aquatic media: simulation of oceanic conditions. **35**, 909–921.

650   Amrani A., Turner J. W., Ma Q., Tang Y. and Hatcher P. G. (2007) Formation of sulfur and nitrogen
651   cross-linked macromolecules under aqueous conditions. *Geochimica et Cosmochimica Acta* **71**,
652   4141–4160.

653   Anderson L. and Sarmiento J. L. (1994) Redfield ratios of remineralization determined by nutrient data
654   analysis. *Global Biogeochemical Cycles* **8**, 65–80.

655   Anderson R., Kates M. and Volcani B. E. (1978) Identification of the sulfolipids in the non-
656   photosynthetic diatom Nitzschia alba. *Marine and Petroleum Geology* **528**, 89–106.

657   Arnarson T. S. and Keil R. G. (2007) Changes in organic matter–mineral interactions for marine
658   sediments with varying oxygen exposure times. *Geochimica et Cosmochimica Acta* **71**, 3545–3556.

659   Arndt S., Jorgensen B. B., LaRowe D. E., Middelburg J. J., Pancost R. D. and Regnier P. (2013)
660   Quantifying the degradation of organic matter in marine sediments: A review and synthesis. *Earth*
661   *Science Reviews* **123**, 53–86.

662   Arnosti C., Wietz M., Brinkhoff T., Hehemann J. H., Probandt D., Zeugner L. and Amann R. (2021) The
663   Biogeochemistry of Marine Polysaccharides: Sources, Inventories, and Bacterial Drivers of the
664   Carbohydrate Cycle. *Annu. Rev. Mar. Sci.* **13**, 81–108.

665   Arthur M. A., Dean W. E. and Pratt L. M. (1988) Geochemical and climatic effects of increased marine
666   organic carbon burial at the Cenomanian/Turonian boundary.

667   Benson A. A., Daniel H. and Wiser R. (1959) a Sulfolipid in Plants. In *Proceedings of the National*
668   *Academy of Sciences of the United States of America.* **45**, 1582–1587.

669   Bhaskar P. V. and Bhosle N. (2005) Microbial extracellular polymeric substances in marine
670   biogeochemical processes. *Journal of Paleontology* **88**, 45–53.

671   Bianchi T. S., Cui X., Blair N. E., Burdige D. J., Eglinton T. I. and Galy V. (2018) Centers of organic
672   carbon burial and oxidation at the land-ocean interface. *Organic Geochemistry* **115**, 138–155.

673   Boulegue J., Lord C. J. III and Church T. M. (1982) Sulfur speciation and associated trace metals (Fe, Cu)
674   in the pore waters of Great Marsh, Delaware. *Marine and Petroleum Geology* **46**, 453–464.

675   Boussafir M. and Lallier-Verges E. (1997) Accumulation of organic matter in the Kimmeridge Clay
676   Formation (KCF): an update fossilisation model for marine petroleum source-rocks. *Marine and*
677   *Petroleum Geology* **14**, 75–83.

678   Boyd P. W., Claustre H., Lévy M., Siegel D. A. and Weber T. (2019) Multi-faceted particle pumps drive
679   carbon sequestration in the ocean. *Nature Publishing Group* **568**, 1–9.

680   Boye K., Noël V., Tfaily M. M., Bone S. E., Williams K. H., Bargar J. R. and Fendorf S. (2017)
681   Thermodynamically controlled preservation of organic carbon in floodplains. *Nature Geosci* **10**,
682   415–419.

683   Braissant O., Decho A. W., Dupraz C., Glunk C., Przekop K. M. and Visscher P. T. (2007) Exopolymeric
684   substances of sulfate-reducing bacteria: Interactions with calcium at alkaline pH and implication for
685   formation of carbonate minerals. *Geobiology* **5**, 401–411.

686   Breitburg D., Levin L. A., Oschlies A., Grégoire M., Chavez F. P., Conley D. J., Garçon V., Gilbert D.,
687   Gutiérrez D., Isensee K., Jacinto G. S., Limburg K. E., Montes I., Naqvi S. W. A., Pitcher G. C.,
688   Rabalais N. N., Roman M. R., Rose K. A., Seibel B. A., Telszewski M., Yasuhara M. and Zhang J.
689   (2018) Declining oxygen in the global ocean and coastal waters. **359**, eaam7240–13.

690   Canfield D. E., Boudreau B. P., Mucci A. and Gundersen J. K. (1998) The early diagenetic formation of
691   organic sulfur in the sediments of Mangrove Lake, Bermuda. *Marine and Petroleum Geology* **62**,
692   767–781.

693   Canfield D. E., Raiswell R. and Bottrell S. H. (1992) The reactivity of sedimentary iron minerals toward
694   sulfide. *American Journal of Science* **292**, 659–683.

695   Canfield D. E., Stewart F. J., Thamdrup B., De Brabandere L., Dalsgaard T., Delong E. F., Revsbech N.
696   P. and Ulloa O. (2010) A Cryptic Sulfur Cycle in Oxygen-Minimum-Zone Waters off the Chilean
697   Coast. *Science* **330**, 1375–1378.

698   Cavan E. L., Trimmer M., Shelley F. and Sanders R. (2017) Remineralization of particulate organic
699   carbon in an ocean oxygen minimum zone. *Nature Communications* **8**, 2077–9.

700   Chen C., Lin C. M., Huang B. T., Chemistry L. C. M.1996 (1996) Stoichiometry of carbon, hydrogen,
701   nitrogen, sulfur and oxygen in the particulate matter of the western North Pacific marginal seas.
702   *Marine and Petroleum Geology* **54**, 179–190.

703   Cuhel R. L., Taylor C. D. and Jannasch H. W. (1982) Assimilatory Sulfur Metabolism in Marine
704   Microorganisms: Sulfur Metabolism, Protein Synthesis, and Growth of Alteromonas luteo-violaceus
705   and Pseudomonas halodurans During Perturbed Batch Growth. *Appl. Environ. Microbiol.* **43**, 151–
706   159.

707   Dale A. W., Bruchert V., Alperin M. and Regnier P. (2009) An integrated sulfur isotope model for
708   Namibian shelf sediments. *Geochimica et Cosmochimica Acta* **73**, 1924–1944.

709   Deutsch C., Brix H., Ito T., Frenzel H. and Thompson L. (2011) Climate-Forced Variability of Ocean
710   Hypoxia. *Science* **333**, 336–341.

711   Devol A. and Hartnett H. E. (2001) Role of the oxygen-deficient zone in transfer of organic carbon to the
712   deep ocean. *Limnology and Oceanography* **46**, 1684–1690.

713   Dunne J. P., Sarmiento J. L. and Gnanadesikan A. (2007) A synthesis of global particle export from the
714   surface ocean and cycling through the ocean interior and on the seafloor. *Global Biogeochemical*
715   *Cycles* **21**, GB4006.

716   Filley T., Freeman K., Wilkin R. and Hatcher P. (2002) Biogeochemical controls on reaction of
717   sedimentary organic matter and aqueous sulfides in Holocene sediments of Mud Lake, Florida.
718   *Geochimica et Cosmochimica Acta* **66**, 937–954.

719   Findlay A. J. (2016) Microbial impact on polysulfide dynamics in the environment ed. R. Boden. *FEMS*
720   *Microbiology Letters* **363**, fnw103–12.

721   Findlay A. J., Pellerin A., Laufer K. and Jorgensen B. B. (2020) Quantification of sulphide oxidation rates
722   in marine sediment. *Geochimica et Cosmochimica Acta*, **280**, 441-452.

723   Francois R. (1987) A study of sulphur enrichment in the humic fraction of marine sediments during early
724   diagenesis. *Geochimica et Cosmochimica Acta* **51**, 17–27.

725   Froelich P. N., Klinkhammer G. P., Bender M. L., Luedtke N. A., Heath G. R., Cullen D. and Dauphin P.
726   (1979) Early oxidation of organic matter in pelagic sediments of the eastern equatorial Atlantic:
727   suboxic diagenesis. *Geochimica et Cosmochimica Acta* **43**, 1075–1090.

728   Gelin F., Kok M. D., De Leeuw J. W. and Damsté J. S. S. (1998) Laboratory sulfurisation of the marine
729   microalga Nannochloropsis salina. **29**, 1837–1848.

730   Gomez-Saez G. V., Niggemann J., Dittmar T., Pohlabeln A. M., Lang S. Q., Noowong A., Pichler T.,
731   Wörmer L. and Bühring S. I. (2016) Molecular evidence for abiotic sulfurization of dissolved organic
732   matter in marine shallow hydrothermal systems. *Geochimica et Cosmochimica Acta* **190**, 35–52.

733   Hartgers W. A., Lopez J. F., Damste J. S., Reiss C., Maxwell J. and Grimalt J. O. (1997) Sulfur-binding
734   in recent environments: II. Speciation of sulfur and iron and implications for the occurrence of
735   organo-sulfur compounds. *Geochimica et Cosmochimica Acta* **61**, 4769–4788.

736   Hartnett H. E. and Devol A. H. (2003) Role of a strong oxygen-deficient zone in the preservation and
737   degradation of organic matter: A carbon budget for the continental margins of northwest Mexico and
738   Washington State. *Geochimica et Cosmochimica Acta* **67**, 247–264.

739   Hayes J. M. (2001) Fractionation of the isotopes of carbon and hydrogen in biosynthetic processes. In
740   National Meeting of the Geological Society of America. Boston, MA.

741   Heller M. I., Lam P. J., Moffett J. W., Till C. P., Lee J.-M., Toner B. M. and Marcus M. A. (2017)
742   Accumulation of Fe oxyhydroxides in the Peruvian oxygen deficient zone implies non-oxygen
743   dependent Fe oxidation. *Geochimica et Cosmochimica Acta* **211**, 174–193.

744   Hill R. L. (1965) Hydrolysis of Proteins. In *Advances in Protein Chemistry Volume 20* Advances in
745   Protein Chemistry. Elsevier. pp. 37–107.

746   Holmkvist L., Ferdelman T. G. and Jorgensen B. B. (2011) A cryptic sulfur cycle driven by iron in the
747   methane zone of marine sediment (Aarhus Bay, Denmark). *Geochimica et Cosmochimica Acta* **75**,
748   3581–3599.

749　Hülse D., Arndt S. and Ridgwell A. (2019) Mitigation of Extreme Ocean Anoxic Event Conditions by
750　　　Organic Matter Sulfurization. *Paleoceanography and Paleoclimatology* **34**, 476–489.

751　Ishizuka I. (1997) Chemistry and functional distribution of sulfoglycolipids. *Marine and Petroleum*
752　　　*Geology* **36**, 245–319.

753　Iversen M. H. and Ploug H. (2013) Temperature effects on carbon-specific respiration rate and sinking
754　　　velocity of diatom aggregates; potential implications for deep ocean export processes.
755　　　*Biogeosciences* **10**, 4073–4085.

756　Jessen G. L., Lichtschlag A., Ramette A., Pantoja S., Rossel P. E., Schubert C. J., Struck U. and Boetius
757　　　A. (2017) Hypoxia causes preservation of labile organic matter and changes seafloor microbial
758　　　community composition (Black Sea). *Science Advances* **3**, e1601897.

759　Johnston D. T., Gill B. C., Masterson A., Beirne E., Casciotti K. L., Knapp A. N. and Berelson W. (2014)
760　　　Placing an upper limit on cryptic marine sulphur cycling. *Nature* **513**, 530-533.

761　Jorgensen B. B. (2019) The Biogeochemical Sulfur Cycle of Marine Sediments. *Frontiers in*
762　　　*Microbiology* **10,** 849.

763　Kamyshny A., Goifman A., Gun J., Rizkov D. and Lev O. (2004) Equilibrium Distribution of Polysulfide
764　　　Ions in Aqueous Solutions at 25 °C: A New Approach for the Study of Polysulfides' Equilibria.
765　　　*Environmental Science and Technology* **38**, 6633–6644.

766　Keil R. G., Neibauer J. A., Biladeau C., van der Elst K. and Devol A. (2016) A multiproxy approach to
767　　　understanding the "enhanced" flux of organic matter through the oxygen-deficient waters of the
768　　　Arabian Sea. *Biogeosciences* **13**, 2077–2092.

769　Kohnen M., Damste J. S., Haven ten H. L. and De Leeuw J. W. (1989) Early incorporation of
770　　　polysulfides in sedimentary organic matter. **341**, 640–641.

771　Kohnen M., Sinninghe, Dalen A. K.-V. and De Leeuw J. W. (1991) Di- or polysulphide-bound
772　　　biomarkers in sulphur-rich geomacromolecules as revealed by selective chemolysis. *Geochimica et*
773　　　*Cosmochimica Acta* **55**, 1375–1394.

774　Kok M. D., Schouten S. and Sinninghe Damsté J. S. (2000) Formation of insoluble, nonhydrolyzable,
775　　　sulfur-rich macromolecules via incorporation of inorganic sulfur species into algal carbohydrates.
776　　　*Marine and Petroleum Geology* **64**, 2689–2699.

777　Kok M., Rijpstra I., Robertson L., Volkman J. K. and Damste J. S. (2000) Early steroid sulfurisation in
778　　　surface sediments of a permanently stratified lake (Ace Lake, Antarctica). *Geochimica et*
779　　　*Cosmochimica Acta* **64**, 1425–1436.

780　Kutuzov I., Rosenberg Y. O., Bishop A. and Amrani A. (2019) The Origin of Organic Sulphur
781　　　Compounds and Their Impact on the Paleoenvironmental Record. In *Hydrocarbons, Oils and Lipids:*
782　　　*Diversity, Origin, Chemistry and Fate* Springer International Publishing, Cham. pp. 1–54.

783　La Rocha De C. L. and Passow U. (2007) Factors influencing the sinking of POC and the efficiency of
784　　　the biological carbon pump. *Deep Sea Research Part II: Topical Studies in Oceanography* **54**, 639–
785　　　658.

786 LaLonde R., Ferrara L. and Hayes M. (1987) Low-temperature, polysulfide reactions of conjugated ene
787   carbonyls: A reaction model for the geologic origin of S-heterocycles. *Organic Geochemistry* **11**,
788   563–571.

789 Li X., Taylor G. T., Astor Y. and Scranton M. I. (2008) Relationship of sulfur speciation to hydrographic
790   conditions and chemoautotrophic production in the Cariaco Basin. *Marine Chemistry* **112**, 53–64.

791 Luther G. W., Church T. M., Scudlark J. R. and Cosman M. (1986) Inorganic and Organic Sulfur Cycling
792   in Salt-Marsh Pore Waters. *Science* **232**, 746–749.

793 Lückge A., Boussafir M., Lallier-Verges E. and Littke R. (1996) Comparative study of organic matter
794   preservation in immature sediments along the continental margins of Peru and Oman. Part I: Results
795   of petrographical and bulk geochemical data. *Organic Geochemistry* **24**, 437–451.

796 Lyons T. W. (1997) Sulfur isotopic trends and pathways of iron sulfide formation in upper Holocene
797   sediments of the anoxic Black Sea. *Geochimica et Cosmochimica Acta* **61**, 3367–3382.

798 Lyons T. W., Reinhard C. T. and Planavsky N. J. (2014) The rise of oxygen in Earth's early ocean and
799   atmosphere. **506**, 307–315.

800 Lyons T. W., Werne J. P., Hollander D. J. and Murray R. W. (2003) Contrasting sulfur geochemistry and
801   Fe/Al and Mo/Al ratios across the last oxic-to-anoxic transition in the Cariaco Basin, Venezuela.
802   *Chemical Geology* **195**, 131–157.

803 Martin J. H., Knauer G. A., Karl D. M. and Broenkow W. (1987) VERTEX: carbon cycling in the
804   northeast Pacific. *Marine and Petroleum Geology* **34**, 267–285.

805 Matrai P. A. and Eppley R. W. (1989) Particulate organic sulfur in the waters of the Southern California
806   Bight. *Global Biogeochemical Cycles* **3**, 89–103.

807 Matrai P. A. and Vetter R. D. (1988) Particulate thiols in coastal waters: The effect of light and nutrients
808   on their planktonic production. *Limnology and Oceanography* **33**, 624–631.

809 Metzger K., Rehberger P. A., Erben G. and Lehmann W. D. (1995) Identification and Quantification of
810   Lipid Sulfate Esters by Electrospray Ionization MS/MS Techniques: Cholesterol Sulfate. *Analytical*
811   *Chemistry* **67**, 4178–4183.

812 Mossman J. R., Aplin A. C., Curtis C. D. and Coleman M. L. (1991) Geochemistry of inorganic and
813   organic sulphur in organic-rich sediments from the Peru Margin. *Geochimica et Cosmochimica Acta*
814   **55**, 3581–3595.

815 Overmann J., Beatty J. T., Krause H. R. and Hall K. J. (1996) The sulfur cycle in the chemocline of a
816   meromictic salt lake. *Limnology and Oceanography* **41**, 147–156.

817 Passow U., Alldredge A. L. and Logan B. E. (1994) The role of particulate carbohydrate exudates in the
818   flocculation of diatom blooms. *Marine and Petroleum Geology* **41**, 335–357.

819 Percival E., Rahman M. A. and Weigel H. (1980) Chemistry of the polysaccharides of the diatom
820   Coscinodiscus nobilis. *Marine and Petroleum Geology* **19**, 809–811.

Phillips A. A., Wu F. and Sessions A. L. (2021) Sulfur isotope analysis of cysteine and methionine via preparatory liquid chromatography and elemental analyzer isotope ratio mass spectrometry. *Rapid Commun. Mass Spectrom.* **35**, 175–24.

Pohlabeln A. M., Gomez-Saez G. V., Noriega-Ortega B. E. and Dittmar T. (2017) Experimental Evidence for Abiotic Sulfurization of Marine Dissolved Organic Matter. *Front. Mar. Sci.* **4**, 265.

Ramus J. and Groves S. T. (1974) Precursor-Product Relationships during Sulfate Incorporation into Porphyridium Capsular Polysaccharide. *Plant Physiology* **53**, 434–439.

Raven M. R., Fike D. A., Bradley A. S., Gomes M. L., Owens J. D. and Webb S. A. (2019) Paired organic matter and pyrite δ34S records reveal mechanisms of carbon, sulfur, and iron cycle disruption during Ocean Anoxic Event 2. *Earth and Planetary Science Letters* **512**, 27–38.

Raven M. R., Fike D. A., Gomes M. L. and Webb S. M. (2019) Chemical and Isotopic Evidence for Organic Matter Sulfurization in Redox Gradients Around Mangrove Roots. *Front. Earth Sci.* **7**.

Raven M. R., Fike D. A., Gomes M. L., Webb S. M., Bradley A. S. and McClelland H.-L. O. (2018) Organic carbon burial during OAE2 driven by changes in the locus of organic matter sulfurization. *Nature Communications* **9**, 3409.

Raven M. R., Keil R. G. and Webb S. M. (2021) Microbial sulfate reduction and organic sulfur formation in sinking marine particles. **371**, 178–181.

Raven M. R., Sessions A. L., Adkins J. F. and Thunell R. C. (2016) Rapid organic matter sulfurization in sinking particles from the Cariaco Basin water column. *Geochimica et Cosmochimica Acta* **190**, 175–190.

Raven M. R., Sessions A. L., Fischer W. W. and Adkins J. F. (2016) Sedimentary pyrite δ34S differs from porewater sulfide in Santa Barbara Basin: Proposed role of organic sulfur. *Geochimica et Cosmochimica Acta* **186**, 120–134.

Resing J. A., Sedwick P. N., German C. R., Jenkins W. J., Moffett J. W., Sohst B. M. and Tagliabue A. (2015) Basin-scale transport of hydrothermal dissolved metals across the South Pacific Ocean. *Nature* **523**, 200–203.

Rickard D. and Luther G. W. (2007) Chemistry of Iron Sulfides. *Chem. Rev.* **107**, 514–562.

Rickard D. and Morse J. (2005) Acid volatile sulfide (AVS). *Marine Chemistry* **97**, 141–197.

Salmon V., Derenne S., Lallier-Verges E., Largeau C. and Beaudoin B. (2000) Protection of organic matter by mineral matrix in a Cenomanian black shale. **31**, 463–474.

Schmidtko S., Stramma L. and Visbeck M. (2017) Decline in global oceanic oxygen content during the past five decades. *Nature* **542**, 335–339.

Sinninghe Damsté J. S., Irene W., Rijpstra C., De Leeuw J. W. and Schenck P. A. (1988) Origin of organic sulphur compounds and sulphur-containing high molecular weight substances in sediments and immature crude oils. *Organic Geochemistry* **13**, 593–606.

856 Sinninghe Damsté J. S. and Köster J. (1998) A euxinic southern North Atlantic Ocean during the
857   Cenomanian/Turonian oceanic anoxic event. *Marine and Petroleum Geology* **158**, 165–173.

858 Stramma L., Prince E. D., Schmidtko S., Luo J., Hoolihan J. P., Visbeck M., Wallace D. W. R., Brandt P.
859   and Körtzinger A. (2011) Expansion of oxygen minimum zones may reduce available habitat for
860   tropical pelagic fishes. *Nature Climate Change* **2**, 33–37.

861 Suits N. S. and Arthur M. A. (2000) Sulfur diagenesis and partitioning in Holocene Peru shelf and upper
862   slope sediments. *Chemical Geology* **163**, 219–234.

863 Takano Y., Ito T. and Deutsch C. (2018) Projected Centennial Oxygen Trends and Their Attribution to
864   Distinct Ocean Climate Forcings. *Global Biogeochemical Cycles* **32**, 1329–1349.

865 Urban N. R., Ernst K. and Bernasconi S. (1999) Addition of sulfur to organic matter during early
866   diagenesis of lake sediments. *Geochimica et Cosmochimica Acta* **63**, 837–853.

867 van de Velde S. J., Reinhard C. T., Ridgwell A. and Meysman F. J. R. (2020) Bistability in the redox
868   chemistry of sediments and oceans. *Proceedings of the National Academy of Sciences* **483**,
869   202008235.

870 van Dongen B. E., Schouten S., Baas M., Geenevasen J. A. J. and Sinninghe Damsté J. S. (2003) An
871   experimental study of the low-temperature sulfurization of carbohydrates. *Organic Geochemistry* **34**,
872   1129–1144.

873 Van Mooy B. A. S. and Keil R. G. (2015) Aquatic sample analysis system. U.S. Patent 9,188,512.

874 Van Mooy B., Keil R. G. and Devol A. H. (2002) Impact of suboxia on sinking particulate organic
875   carbon: Enhanced carbon flux and preferential degradation of amino acids via denitrification.
876   *Geochimica et Cosmochimica Acta* **66**, 457–465.

877 Vidal-Melgosa S., Sichert A., Ben Francis T., Bartosik D., Niggemann J., Wichels A., Willats W. G. T.,
878   Fuchs B. M., Teeling H., Becher D., Schweder T., Amann R. and Hehemann J.-H. (2021) Diatom
879   fucan polysaccharide precipitates carbon during algal blooms. *Nature Communications* **12**, 1150.

880 Vogt W. (1995) Oxidation of methionyl residues in proteins: tools, targets, and reversal. *Marine and*
881   *Petroleum Geology* **18**, 93–105.

882 Webb S. M. (2005) SIXpack: a graphical user interface for XAS analysis using IFEFFIT. *Phys. Scr.* **2005**,
883   1011.

884 Webb S. M., McNulty I., Eyberger C. and Lai B. (2011) The MicroAnalysis Toolkit: X-ray Fluorescence
885   Image Processing Software. In the 10th International Conference on X-ray Microscopy. AIP. pp.
886   196–199.

887 Werne J. P., Lyons T. W., Hollander D. J., Chemical M. F. and Sinninghe Damsté J. S. (2003) Reduced
888   sulfur in euxinic sediments of the Cariaco Basin: sulfur isotope constraints on organic sulfur
889   formation. *Marine and Petroleum Geology* **195**, 159–179.

890 Werne J., Hollander D., Behrens A., Schaeffer P., Albrecht P. and Damste J. (2000) Timing of early
891   diagenetic sulfurization of organic matter: A precursor-product relationship in early Holocene

892   sediments of the anoxic Cariaco Basin, Venezuela. *Geochimica et Cosmochimica Acta* **65**, 1741–
893   1751.

894   Zerkle A., Kamyshny A., Kump L., Farquhar J., Oduro H. and Arthur M. (2010) Sulfur cycling in a
895   stratified euxinic lake with moderately high sulfate: constraints from quadruple S isotopes.
896   *Geochimica et Cosmochimica Acta* **74**, 4953–4970.

897